Available online at www.sciencedirect.com
ScienceDirect
Microelectronics Reliability 48 (2008) 68–82
MICROELECTRONICS RELIABILITY
www.elsevier.com/locate/microrel

A strategy for damage assessment of thermally stressed copper vias in microelectronic printed circuit boards

K. Weinberg *, W.H. Müller

Technische Universität Berlin, Institut für Mechanik, Einsteinufer 5, 10587 Berlin, Germany

Received 11 January 2006; received in revised form 23 February 2007
Available online 9 May 2007

Abstract

The thermal fatigue of plated-through vias remains a subject of concern, particularly when exposed to the high operating temperatures associated with automotive applications. In this paper the performance of different types of copper vias in different positions of a printed circuit board is analyzed. To this end a two-scale finite element analysis under the loading conditions of thermal cycling is employed. A new material model for the electrolytically deposited copper accounts for large elastic and plastic deformations and, additionally, for the growth of pores within the material.

It is common practice to extrapolate the plastic straining computed within few steps of thermal cycling by means of a Coffin–Manson-Equation. We critical examine this strategy and point out, that a certain number of about 20 cycling steps is necessary to obtain meaningful extrapolations. Furthermore, an extrapolation of the computed porosity up to critical values allows similar conclusions.

The presented strategy can serve as a predictive tool for plated through holes and vias and can reduce the need of repetitive experimental failure tests.

1. Introduction

Plated-through holes and vias form conductive paths between the different copper layers of circuit boards, see Fig. 1. Failure of these connectors due to thermomechanical stresses is a well established cause of failure of circuit boards. Therefore, life expectation of plated through vias is of great interest for the microelectronic industry.

Vias are commonly made of (electrolytically deposited) copper whereas the surrounding material is typical a non-isotropic resin, e.g., the glass fibre reinforced resin FR4 (flame-retardant 4 material substrate), [12]. To ensure the required life expectation of circuit units standarized thermal cycle tests are performed. Due to the different thermal expansion coefficients of the copper and the anisotropic board the copper vias are highly stressed and strained. This leads to an accumulation of permanent irreversible strains associated with cracks and pores which eventually results in the electro-mechanical destruction of the connector.

In this paper we will present a numerical study of such copper vias subjected to thermal cycling between −40 °C and +150 °C (automotive standard, see Fig. 2). After introducing a general technique of how to analyze the stress state in small chip components we focus on a new material model accounting for both, plastic straining and the growth of pores and voids within the copper via. We estimate the damage for vias with different fillings and in different positions in an FR4 board onto which a flip chip component has been mounted (FCOB = Flip Chip On Board) and we suggest a technique for improved life time estimation.

2. Finite-element modelling of the circuit board and the plated-through vias

High density interconnect (HDI) technology is an advanced packaging technology enabling more and more

* Corresponding author. Tel.: +49 30 314 24214; fax: +49 30 314 24499.
E-mail address: weinberg@mech2.pi.tu-berlin.de (K. Weinberg).

0026-2714/$ - see front matter © 2007 Elsevier Ltd. All rights reserved.
doi:10.1016/j.microrel.2007.03.003

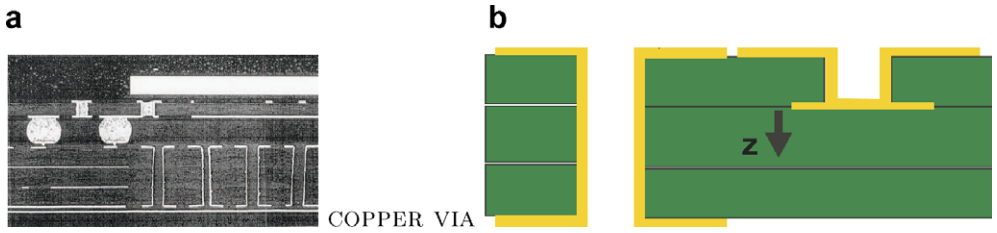

Fig. 1. Board and SMT components in the cross section of a microchip: (a) HDI components, cf. [11]; (b) schematics of plated-through via and microvia.

functions to be utilized in a smaller area for, e.g., the next generation of small portable electronic communication devices. HDI technology is based on various types of build up methods for the manufacture of multi-layer Printed-Circuit boards (PC boards). Fig. 1 illustrates the principle setup of a PC board with plated-through holes, vias and microvias, where the main physical difference between the first two is the diameter of the hole. A plated-through-hole is usually made to have a wire or a lead of a component soldered into it. After plating the inner diameter of the hole is sized such as to receive a wire with sufficient clearance. A via is a special kind of plated through holes that is not intended to contain a wire but simply to provide a conductive path from one copper layer to another. Thus, its hole diameter is usually much smaller. A microvia is an even smaller connection to attach solder balls to the copper layer structure on the PC board (right hand side of Fig. 1b). Microvias can be studied in a manner completely analogous to the one presented here for vias.

Note that the issue of filling the plated-through vias with solder or epoxy and, if possible, to increase its life expectation as opposed to leaving it unfilled has been open to considerable debate, see, e.g., [3].

Compared to a PC board and the microelectronic components mounted thereon the plated-through vias and microvias are much smaller. If modelled directly this would lead to a finite-element mesh with an unnecessarily high amount of degrees of freedom. For that reason we make use of a submodelling technique. This is a two-step procedure during which a global model is created first. In the

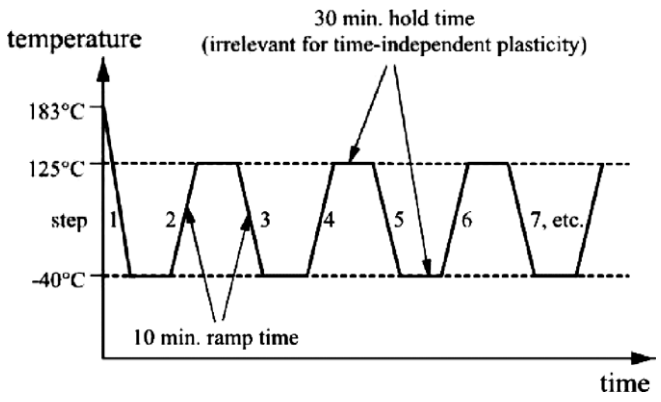

Fig. 2. Temperature cycling between −40 °C and 150 °C.

presented case the global model consists of the chip (more precisely: the FCOB unit) and of the PC board, for dimensions see Fig. 3. Note that delicate substructures, such as the vias, are not included. Moreover, by symmetry the finite-element mesh is reduced to one quarter of chip and board. A finite-element analysis is then performed with this model, i.e., temperature cycles between −40 °C and 150 °C are imposed (233/423 K), see Fig. 2, where the first step describes the cooling down from the melting temperature of SnPb solder of 183 °C. From the global structure the locally resulting stresses, strains, and deformations are calculated.

In a second step finite-element submodels of the structures of interest, namely the plated-through vias, are created in a way that the geometry of the real objects is reflected in a sufficiently accurate manner. The deformations at selected positions that result from the finite-element calculation of the global model are now extrapolated and imposed onto the periphery of the local models. Thus, the mechanical response within the substructures can be calculated. Note that here the reaction of the submodel to the global structure is considered to be negligible small. If the influence of the plated-through vias on the global structure is of interest, homogenization techniques are required, as, e.g., suggested in [6]. Clearly, it is desirable that during the finite-element analysis (FEA) the stresses and strains are as accurately calculated as possible. Therefore, special attention must be paid to the generation of the submodel meshes so that all regions of interest, in the present case the copper, are sufficiently far away from the boundary of the submodel.

The global model essentially consist of an chip mounted upon a PC board. The board is made of FR4, a special resin with high glass-transition temperature and with orthotropic (transversal isotropic) material properties, see Table 4 in the Appendix. In order to avoid the aforementioned numerical inaccuracy problems in context with the submodels, i.e., in order not to use submodels that show copper structures upon their surfaces a quarter of the whole structure was modelled. Symmetry conditions were imposed along the *diagonal* surfaces. Moreover, it was made sure that the front surface of the compound consisting of solder stop mask and PC-board did not tilt but rather moved in a straight manner in order to mimic the embodiment of the package within the whole assembly.

A submodel for the straight-through via is shown in Fig. 4. Note that the copper part is also completely

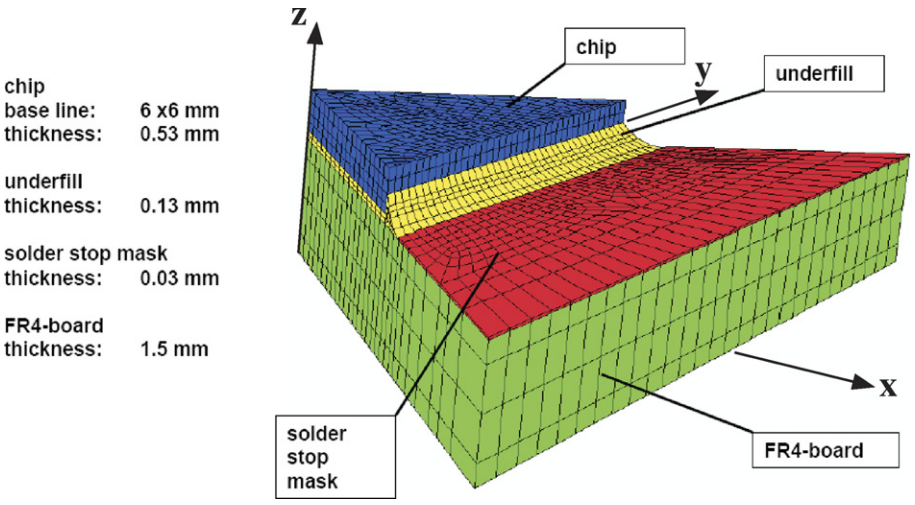

Fig. 3. Finite-element model of a FCOB circuit unit.

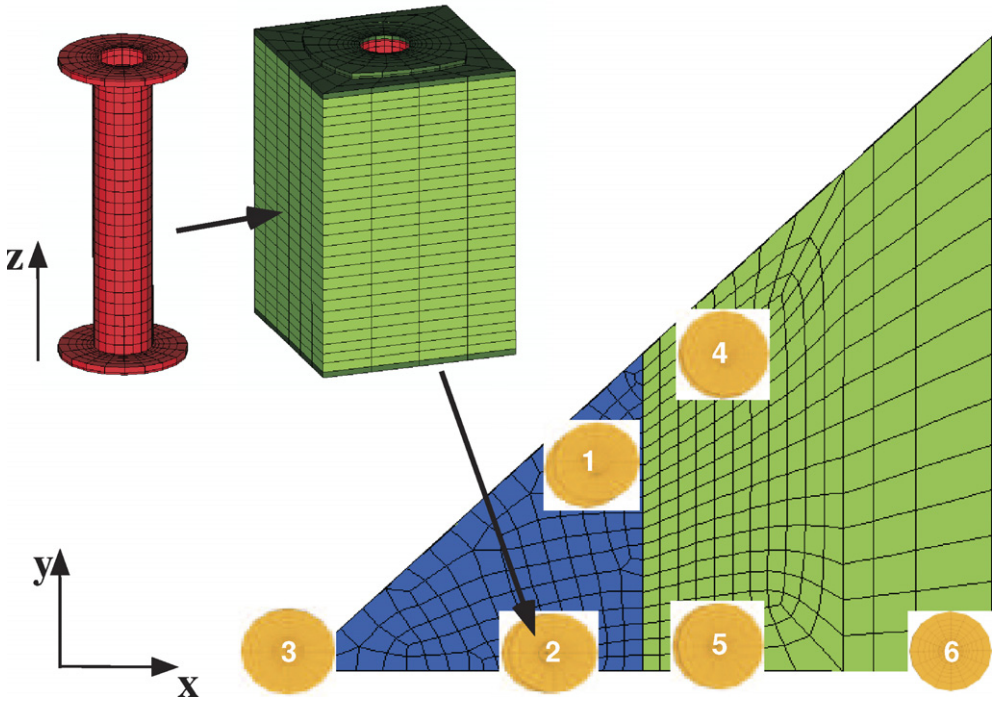

Fig. 4. Positions of the vias within the global structure.

Table 1
Positions of the vias

Via	1	2	3	4	5	6
x (mm)	1.5	0.0	0.0	2.91	0.0	0.0
y (mm)	2.5	2.35	1.0	4.0	4.0	4.8

surrounded by underfill, solder stop mask and PC board material. The submodels were positioned at various points of the board, see Table 1. For reasons of conciseness only one eighth of the whole structure is shown in Fig. 4 with the out-of plane direction being the z-axis. However, all submodels, also those along the horizontal line, i.e., the y-axis, are completely embedded in the global model.

The dimensions of the plated-through vias are as follows: width of the basal plane of the whole submodel 1.0 mm, wall thickness of the copper cylinder 0.022 mm, inner diameter 0.256 mm, outer diameter 0.65 mm, height of the submodel 1.5 mm. At the upper and the lower surface the copper via is covered by a thin layer of solder stop mask with material parameters of Table 5; the copper structure is surrounded by the orthotropic FR4 resin (cf. Fig. 4).

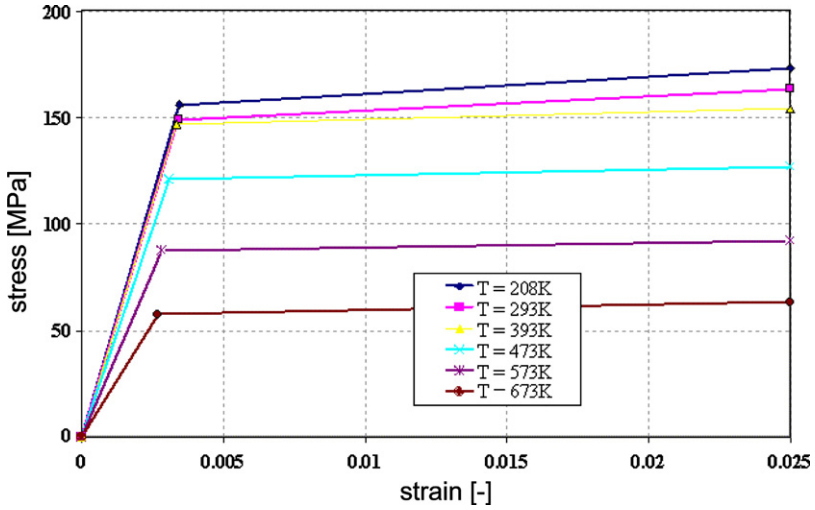

Fig. 5. Stress–strain curves for electrodeposited copper provided by [5].

During the manufacturing of plated-through vias and other electrical connectors in high-density-substrates the copper is electrolytically deposited, hence, the mechanical properties may differ significantly from those of bulk copper. Stress–strain curves for electrolytically deposited copper are rarely provided in the literature with data depending on temperature. The presented finite-element simulations make use of the material data shown in Fig. 5. These bilinear stress–strain diagrams were published by DiTomaso [5], obtained from data provided by IBM electronics division at Endicott, NY, based upon in-house testing of electrodeposited copper. The corresponding thermal expansion coefficient is $\alpha = 17.6$ ppm/K. At all the temperatures shown in Fig. 5 an initial yield stress is marked at the end of a linear-elastic branch. This is then followed by hardening up to strains of $\varepsilon = 0.025$. Here we use the measured data of [5] but model the stress–strain curves with a smoother elastic–plastic transition applying a power law of the form

$$\sigma_y = \sigma_{y_0}(T)\left(1 + \frac{\varepsilon^{\mathrm{p}}}{\varepsilon_0^{\mathrm{p}}(T)}\right)^{1/n}. \tag{1}$$

The functions of the initial yield stress $\sigma_y(T)$ and of the reference plastic strain $\varepsilon_0^{\mathrm{p}}(T)$ account for the temperature dependency of plasticity, the hardening exponent is assumed constant with $n = 25$, cf. Table 5.

The material data of [5] describe a very soft material behavior, with an elastic modulus in the range of 40,000 MPa and an initial yield stress of 150 MPa and lower, see Fig. 5. Different but only qualitative observations are reported in [8,13] stating that electrodeposited copper has a higher tensile strength than bulk copper. Read et al. [17] observe in electrodeposited copper films material properties of the same range as typical bulk copper, i.e., $E \approx 120$ GPa and initial yield stresses of $\approx$250 MPa, whereas Lu et al. [9] measure initial yield stresses from of 250–500 MPa up to 1000 MPa depending on the microstructure of the electrodeposited copper. Atomic-scale numerical simulations of nano-crystalline copper in [18] even yield, depending on temperature and grain size, to initial yield stresses of 0.8–1.5 GPa. Unfortunately, none of the other sources provide such detailed information about the temperature dependency of material data as [5].

In Fig. 6 the von Mises stress in the deformed board after cooling to a minimum temperature is shown, with the red and grey colored regions referring to the maxima (of 150...460 MPa) and blue marking the nearly unstressed regions. The warpage of the global structure is magnified by a factor of 50. It can clearly be seen that the highest deformations is along the diagonal surfaces, whereas in the vicinity of via position 4 the highest stresses occur. Depending on the position within the board the warpage will directly influence the deformations of the submodels. Anticipated from the global model in the via positions 1, 2, 4 and 5 shearing deformation appears to be dominant whereas in positions 3 and 6 the via will essentially be stretched. Note that the viscous properties of the materials are not modelled, therefore, the computed deformation can considered to be an upper bound of the actual deformation.

3. Material model for the electrolytically deposited copper

Most metals and alloys contain a certain amount of cavities. These can be defects in the crystal lattice, along grain boundaries or simply vacancies arising during manufacturing. Typically the size of the cavities is small compared to the size of the structure. Their amount is measured by pore volume fraction or porosity

$$f_V = \frac{\text{volume of pores}}{\text{total volume}}. \tag{2}$$

For typical engineering materials the pore volume fraction is initially in the range of 10^{-2} to 10^{-4}. By the technique of electrolytically depositing copper the initial porosity is expected to be higher (cf. [14]), but exact data are not

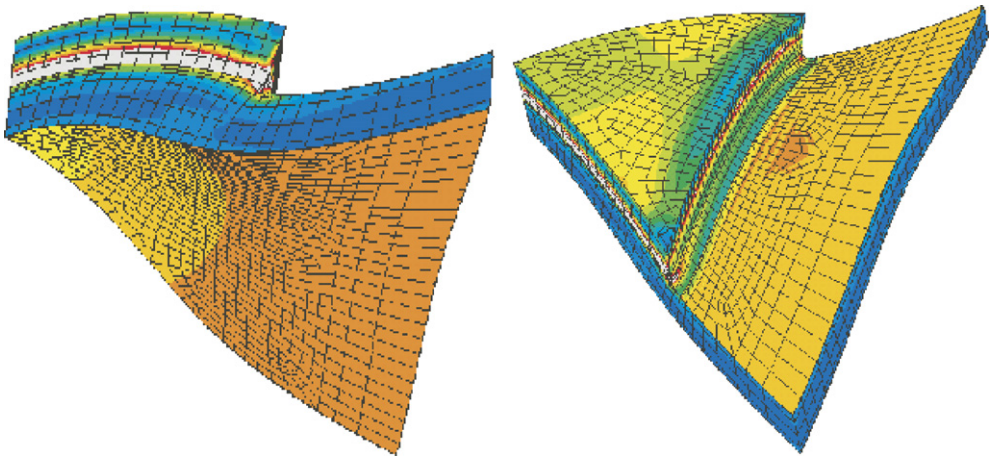

Fig. 6. Von Mises stress in the deformed PC board model. (For interpretation of the references in color in this figure legend, the reader is referred to the web version of this article.)

available. The growth and finally coalescence of these pores in the highly strained material is the basic failure mechanism in ductile fracture, see, e.g., [19] for a review on this subject.

To account for both damaging mechanisms, shear induced plastic straining and growing porosity in the copper material, we employ here a material model that combines classical von Mises plasticity with plastic volumetric expansion as induced by the growth of pores. To this end we postulate the thermo-mechanical response of the material class considered here to be characterized by a free-energy density per unit reference volume of the form

$$A = A(T, \boldsymbol{F}, \boldsymbol{F}^{\mathrm{p}}, \varepsilon^{\mathrm{p}}, \vartheta^{\mathrm{p}}), \tag{3}$$

where T is the absolute temperature, $\boldsymbol{F}$ denotes the deformation gradient whereas $\boldsymbol{F}^{\mathrm{p}}$ (and $\boldsymbol{F}^{\mathrm{e}}$) denote the plastic (and elastic) part of the deformation gradient. Both components are related as follows:

$$\boldsymbol{F} = \boldsymbol{F}^{\mathrm{e}}\boldsymbol{F}^{\mathrm{p}}. \tag{4}$$

Moreover, the internal variable ε^{p} describes the effective plastic straining whereas ϑ^{p} measures the effective volumetric plastic expansion.

Note that we account in this material model for the full kinematics of large deformations. By the use of logarithmic and exponential mappings the subsequent equations can in part be written in the more familiar terms of strain tensor $\boldsymbol{\epsilon}$ with elastic and plastic components $\boldsymbol{\epsilon}^{\mathrm{e}}$ and $\boldsymbol{\epsilon}^{\mathrm{p}}$, respectively. To this end we define

$$\boldsymbol{\epsilon} = \frac{1}{2}\ln(\boldsymbol{F}^{\top}\boldsymbol{F}) \tag{5}$$

and

$$\boldsymbol{\epsilon}^{\mathrm{e}} = \frac{1}{2}\ln(\boldsymbol{F}^{\mathrm{e}\top}\boldsymbol{F}^{\mathrm{e}}) \quad \text{and} \quad \boldsymbol{\epsilon}^{\mathrm{p}} = \frac{1}{2}\ln(\boldsymbol{F}^{\mathrm{p}\top}\boldsymbol{F}^{\mathrm{p}}) \tag{6}$$

to obtain with (4) the additive decomposition

$$\boldsymbol{\epsilon} = \boldsymbol{\epsilon}^{\mathrm{e}} + \boldsymbol{\epsilon}^{\mathrm{p}}. \tag{7}$$

Formulations based on logarithmic elastic strains effectively reduce finite-deformation computations to small-strain updates and pre- and post-processing steps which are purely kinematic and, therefore, material-independent, [10,16].

In general the material response is time-dependent. Here the speed of loading is slow (in the range of several minutes) and therefore strain rate effects are of minor influence. On the other hand, creep effects might play a role. The proper criterium to apply in that case is the so-called homologous temperature, i.e., the current temperature divided by the melting temperature of the material (in K). Creep shall dominate at homologous temperatures above 0.5 but with a melting temperature of about 1300 K copper has for the temperature range of interest in this paper a homologous temperature $\leqslant 0.3$. Therefore, for the calculation of the irreversible deformation in copper creep will be neglected and we proceed to establish a time-independent material model.

We assume that the free-energy density (3) has the additive structure

$$A(\boldsymbol{F}, \boldsymbol{F}^{\mathrm{p}}, \varepsilon^{\mathrm{p}}, \vartheta^{\mathrm{p}}, T) = W^{\mathrm{e}}(\boldsymbol{F}^{\mathrm{e}}, T) + W^{\mathrm{p}}(\varepsilon^{\mathrm{p}}, \vartheta^{\mathrm{p}}, T), \tag{8}$$

where $W^{\mathrm{e}}(\boldsymbol{F}^{\mathrm{e}}, T)$ and $W^{\mathrm{p}}(\varepsilon^{\mathrm{p}}, \vartheta^{\mathrm{p}}, T)$ are the elastic and stored plastic (i.e., dissipated) energy densities per unit undeformed volume, respectively. The elastic strain-energy density may alternatively be expressed in terms of the logarithmic elastic strains (5),

$$W^{\mathrm{e}} \equiv W^{\mathrm{e}}(\boldsymbol{\epsilon}^{\mathrm{e}}, T) = W^{\mathrm{e,vol}}(\mathrm{tr}\boldsymbol{\epsilon}^{\mathrm{e}}, T) + W^{\mathrm{e,dev}}(\mathrm{dev}\,(\boldsymbol{\epsilon}), T), \tag{9}$$

where we split the energy density into a volumetric component and a shear deformation controlled deviatoric component. The corresponding deviatoric part of the strains results from the decomposition

$$\mathrm{dev}\,\boldsymbol{\epsilon} = \boldsymbol{\epsilon} - \frac{1}{3}\boldsymbol{I}\,\mathrm{tr}\boldsymbol{\epsilon} \quad \text{with} \quad \mathrm{tr}\boldsymbol{\epsilon} = \epsilon_{11} + \epsilon_{22} + \epsilon_{33}. \tag{10}$$

The volumetric energy component $W^{\mathrm{e,vol}}$ implies the equation of state of the material, i.e, $p = K\,\mathrm{tr}\boldsymbol{\epsilon}^{\mathrm{e}} - 3\alpha(T - T_0)$,

where $K = E/(3(1-2\nu))$ is the elastic bulk modulus of the material, and α is the thermal expansion coefficient. The deviatoric component $W^{\mathrm{e,dev}}$ is related to the shear modulus $\mu = 2E/(1+\nu)$. Then, with mass density ϱ_0 and specific heat per unit mass c_v the elastic energy density reads

$$W^{\mathrm{e}} = \frac{1}{2}K(\mathrm{tr}\boldsymbol{\epsilon}^{\mathrm{e}} - 3\alpha(T-T_0))^2 + \varrho_0 c_v T\left(1 - \ln\frac{T}{T_0}\right) + \frac{2}{3}\mu|\mathrm{dev}\,\boldsymbol{\epsilon}^{\mathrm{e}}|^2. \tag{11}$$

Following the classical thermo-mechanical approach the stresses can be computed from the derivative of the energy density with respect to the conjugate deformation variable. In particular, the von Mises (or effective deviatoric) stress σ_v is determined by the relation

$$\sigma_v = -\frac{\partial W^{\mathrm{e}}}{\partial \varepsilon^{\mathrm{p}}}(\boldsymbol{\epsilon}^{\mathrm{e}}, T) \tag{12}$$

whereas the pressure is recovered as

$$p = -\frac{\partial W^{\mathrm{e}}}{\partial \vartheta^{\mathrm{p}}}(\boldsymbol{\epsilon}^{\mathrm{e}}, T). \tag{13}$$

The dependence of the elastic energy density W^{e} on the plastic variables ε^{p} and ϑ^{p} is a consequence of the (prior solution unknown) decomposition (7).

The rate of plastic deformation is assumed to obey a flow rule of the form

$$\dot{\boldsymbol{F}}^{\mathrm{p}}\boldsymbol{F}^{\mathrm{p}-1} = \dot{\varepsilon}^{\mathrm{p}}\boldsymbol{M} + \dot{\vartheta}^{\mathrm{p}}\boldsymbol{N}, \tag{14}$$

where the tensors $\boldsymbol{M}$ and $\boldsymbol{N}$ set the direction of the deviatoric and volumetric plastic deformation rates, respectively. The tensor $\boldsymbol{M}$ is assumed to be trace-free and normed, i.e.,

$$\mathrm{tr}\boldsymbol{M} = 0 \quad \text{and} \quad |\boldsymbol{M}|^2 = \frac{3}{2}, \tag{15}$$

whereas the tensor $\boldsymbol{N}$ is allowed to take one of two values,

$$\boldsymbol{N} = \pm\frac{1}{3}\boldsymbol{I}, \tag{16}$$

with the plus sign corresponding to plastic volumetric expansion (pore growth), and the minus sign to plastic compression (pore collapse). The tensors $\boldsymbol{M}$ and $\boldsymbol{N}$ are otherwise unknown and are to be determined as part of the solution. The constraints (15) and (16) may be regarded as defining the assumed kinematics of plastic deformation. The rates of the internal variables $\dot{\varepsilon}^{\mathrm{p}}$ and $\dot{\vartheta}^{\mathrm{p}}$ describe plasticity due to deviatoric straining and volumetric expansion. They are subject to the irreversibility constraints

$$\dot{\varepsilon}^{\mathrm{p}} \geqslant 0 \quad \text{and} \quad \dot{\vartheta}^{\mathrm{p}} \geqslant 0. \tag{17}$$

The stored plastic energy density per unit volume follows from the rate of plastic straining by (cf. [15])

$$\int_0^t \sigma_y \dot{\varepsilon}^{\mathrm{p}}\,\mathrm{d}t = \int_0^{\varepsilon^{\mathrm{p}}} \sigma_y\,\mathrm{d}\varepsilon^{\mathrm{p}}. \tag{18}$$

The deviatoric part of the plastic energy density is constructed to prescribe power-law hardening of the yield stress σ_y according to Eq. (1). This gives

$$W^{\mathrm{p,dev}} \equiv W^{\mathrm{p,dev}}(\varepsilon^{\mathrm{p}}, T) = \frac{n\sigma_y(T)\varepsilon_0^{\mathrm{p}}(T)}{n+1}\left(1 + \frac{\varepsilon^{\mathrm{p}}}{\varepsilon_0^{\mathrm{p}}}\right)^{\frac{n+1}{n}}. \tag{19}$$

The volumetric component $W^{\mathrm{p,vol}} = W^{\mathrm{p,vol}}(\vartheta^{\mathrm{p}}, T)$ will be specified in detailed below. Then, the deviatoric yield stress reduces to

$$\sigma_y = \frac{\partial W^{\mathrm{p}}}{\partial \varepsilon^{\mathrm{p}}}(T, \varepsilon^{\mathrm{p}}, \vartheta^{\mathrm{p}}), \tag{20}$$

and, likewise, the critical cavitation pressure is

$$p_y = \frac{\partial W^{\mathrm{p}}}{\partial \vartheta^{\mathrm{p}}}(T, \varepsilon^{\mathrm{p}}, \vartheta^{\mathrm{p}}). \tag{21}$$

Summarizing the thermo-mechanical framework we define the thermodynamic force Y conjugate to the internal variable ε^{p} as

$$Y = -\frac{\partial A}{\partial \varepsilon^{\mathrm{p}}} = \sigma_v - \sigma_y, \tag{22}$$

where the effective deviatoric stress and the yield stress are given by (12) and (20), respectively. With pressure (13) and (21) the thermodynamic force Z conjugate to the internal variable ϑ^{p} takes the form

$$Z = -\frac{\partial A}{\partial \vartheta^{\mathrm{p}}} = p - p_y. \tag{23}$$

Up to here the components of the free-energy density function coincide with established theories of elasto-plasticity extended to the finite range. The goal of the remaining paragraph is to relate the continuum measures of volumetric deformation to the materials porosity. Through this connection we deduce the stored plastic energy function from the analysis of an ensemble of voids. For simplicity, we assume a dilute distribution of spherical voids each surrounded by a spherical shell of material. This is, of course, a very simplified approach but it enables us to deduce the properties of the void ensemble from the behavior of a single void. For shear-dominated loading conditions the actual void shape may significantly deviate from a spherical symmetry, cf. [7]. For a detailed discussion of this model and a comparison with other approaches we refer to [20].

Consider a representative volume of material of undeformed volume V_0 and deformed volume V, where here and subsequently the subindex 0 designates fields defined on the undeformed configuration. The volumes V_0 and V are related by $V = JV_0$, where

$$J \equiv \det\boldsymbol{F} = \det(\boldsymbol{F}^{\mathrm{e}}\boldsymbol{F}^{\mathrm{p}}) = J^{\mathrm{e}}J^{\mathrm{p}} \tag{24}$$

is the local Jacobian of the deformation and J^{e} and J^{p} are the corresponding elastic and plastic parts. We recall that J^{p} is the ratio of the volumes of infinitesimal material neighborhoods in plastically-deformed setting reference setting. In standard theory of plasticity the solid is not

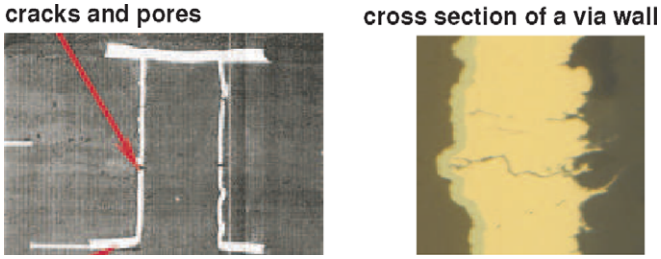

Fig. 7. Stressed vias, studied experimentally in [2].

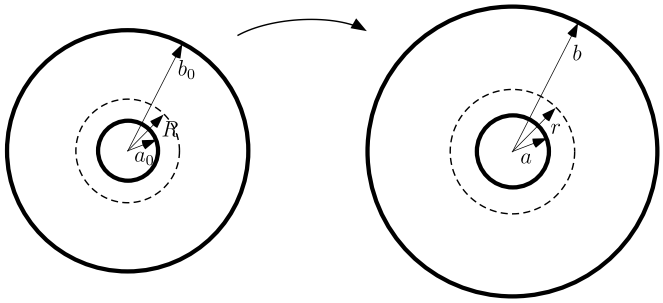

Fig. 8. Spherical shell model of pore growth.

assumed to expand (or compress) plastically, i.e., $J^{\mathrm{p}} \equiv 1$. Alternatively we formulate here

$$J^{\mathrm{p}} = \frac{V}{J^{\mathrm{e}} V_0} \tag{25}$$

to explicitly allow for plastic volumetric expansion of the material.

For further analysis we assume a spherical shell model, i.e., the material is modelled as a conglomerate of (initially very small) spherical voids each surrounded by a sphere of matrix material, see Fig. 8. The voids may grow but retain shape whereas the matrix material follows classical metal elasto-plasticity, i.e., it is incompressible during plastic straining. The volume of undeformed matrix material is $(1 - f_{V0})V_0$. Let us now define the current mean void radius $\bar{a} \equiv \bar{a}(t)$. Then, neglecting the elastic volume change of the voids we can write for the plastic Jacobian (25) of a body with N voids per volume

$$J^{\mathrm{p}} = 1 - f_{V0} + N\frac{4\pi\bar{a}^3}{3}, \tag{26}$$

or, equivalently, in terms of the current void volume fraction

$$f_V = \frac{f_{V0} + J^{\mathrm{p}} - 1}{J^{\mathrm{p}}}. \tag{27}$$

These relations place the mean void radius $\bar{a}$ and J^{p} in one-to-one correspondence. In all subsequent expressions, we conventionally take J^{p} to be the primary independent variable and regard $\bar{a}$, and its functions, as functions of J^{p} through (26).

From the plastic incompressibility constraint (for the matrix material) we know that for any radius r of a material sphere surrounding a void and undergoing with the solid plastic deformation holds

$$\frac{\mathrm{d}}{\mathrm{d}t}\frac{4\pi(r^3 - \bar{a}^3)}{3} = 0. \tag{28}$$

This uniquely determines the velocity over the current configuration (cf. [15])

$$\dot{r} = \frac{\bar{a}^2}{r^2}\dot{\bar{a}}, \tag{29}$$

and the corresponding rate of the effective von Mises strain is

$$\dot{\varepsilon}^{\mathrm{p}}(r,t) = \left|\frac{\partial \dot{r}}{\partial r}\right| = \frac{2\bar{a}^2(t)}{r^3(t)}|\dot{\bar{a}}(t)|. \tag{30}$$

With the incompressibility constraint (28) we can express the current radius r by $r^3 = r_0^3 - a_0^3 + \bar{a}^3$. Integrating (30) in time yields to the plastic strain

$$\begin{aligned}\varepsilon^{\mathrm{p}} &= \frac{2}{3}\ln\left(1 + \frac{\bar{a}^3 - a_0^3}{r^3 - (\bar{a}^3 - a_0^3)}\right)\\ &= \frac{2}{3}\ln\left(1 + \frac{\bar{a}^3 - a_0^3}{r_0^3}\right).\end{aligned} \tag{31}$$

The stored energy function $W^{\mathrm{p}}(\varepsilon^{\mathrm{p}}, \vartheta^{\mathrm{p}}, T)$ is formulated by assuming an additive decomposition into deviatoric and volumetric components and the first part given by (19) models a conventional power law of hardening for the matrix material surrounding the voids. The stored energy for a spherical void in a power-law hardening material equals the plastic work of deformation attendant to the expansion of the void, and, in the dilute limit, the total energy stored by the void ensemble is the sum of the energy stored by each individual void. These considerations applied to a spherical shell model lead by direct calculation from (18) to the stored energy of volumetric plastic work

$$W^{\mathrm{p,vol}}(\bar{a}, T) = N\int_a^b \frac{n\sigma_0(T)\varepsilon_0^{\mathrm{p}}}{n+1}\left(1 + \frac{\varepsilon^{\mathrm{p}}}{\varepsilon_0^{\mathrm{p}}}\right)^{\frac{n+1}{n}} 4\pi r^2\,\mathrm{d}r. \tag{32}$$

Imagine now for a moment a purely volumetric deformation of the body, i.e., the deformation gradient is of the spherical form $\boldsymbol{F} = J^{1/3}\boldsymbol{I}$. Then the flow rule (14) reduces to $\ln(J^{\mathrm{p}})\boldsymbol{I} = \vartheta^{\mathrm{p}}\boldsymbol{N}$ which is evaluated to

$$\frac{\mathrm{d}}{\mathrm{d}t}\ln(J^{\mathrm{p}}) = \mathrm{tr}\boldsymbol{N}\dot{\vartheta}^{\mathrm{p}} = \pm\dot{\vartheta}^{\mathrm{p}}, \tag{33}$$

where the plus sign corresponds to void expansion and the minus sign to void collapse. From (33) we find

$$\dot{\vartheta}^{\mathrm{p}} = \left|\frac{\mathrm{d}}{\mathrm{d}t}\ln J^{\mathrm{p}}\right| \quad \text{and} \quad \vartheta^{\mathrm{p}}(t) = \vartheta^{\mathrm{p}}(0) + \int_0^t \dot{\vartheta}^{\mathrm{p}}(\xi)\,\mathrm{d}\xi, \tag{34}$$

i.e., the variable ϑ^{p} is a measure of the *accumulated* volumetric plastic deformation. Evidently, ϑ^{p} and $\ln J^{\mathrm{p}}$ coincide up to a constant for monotonic expansion. In this case we put

$$\vartheta^{\mathrm{p}} = \ln J^{\mathrm{p}} \tag{35}$$

and with (25) the logarithmic plastic volumetric expansion ϑ^{p} can be expressed as a simple function of mean radius $\bar{a}(t)$

$$\vartheta^{\mathrm{p}} \equiv \vartheta^{\mathrm{p}}(\bar{a}(t)) = \ln\left(1 + \frac{4\pi}{3} N\left(\bar{a}^3(t) - a_0^3\right)\right). \tag{36}$$

Then the stored energy of volumetric plastic work can be formulated as

$$W^{\mathrm{p,vol}}(\vartheta^{\mathrm{p}}, T) = \frac{n\sigma_0(T)\varepsilon_0^{\mathrm{p}}}{n+1} N \frac{4\pi\bar{a}^3}{3} g(\vartheta^{\mathrm{p}}, n), \tag{37}$$

with

$$g(\vartheta^{\mathrm{p}}, n) = \int_1^{\frac{1}{f_V}} \left(1 + \frac{2}{3\varepsilon_0^{\mathrm{p}}} \ln \frac{x}{x - 1 + \frac{f_{V0}}{f_{V0} + \exp \vartheta^{\mathrm{p}} - 1}}\right)^{\frac{n+1}{n}} \mathrm{d}x. \tag{38}$$

Note that these relations hold for arbitrary plastic deformation of the matrix material. In an analogous manner additional energy contributions, e.g., the kinetic energy of the body attributed to pore expansion, can be computed [21].

For an arbitrary loading combining alternating phases of pore expansion and collapse the distinction between the two variables J^{p} and ϑ^{p} becomes important. The simple one-to-one relations (35) and (36) do not hold anymore. For instance, suppose now that the pore radius history $\bar{a}(t)$ grows monotonically from a_0 to $\bar{a}_1$, then decreases montonically from $\bar{a}_1$ to $\bar{a}_2$, and so on. Then the integration of (30) with respect to time gives

$$\begin{aligned}\varepsilon^{\mathrm{p}}(r_0, t) = {} & \frac{2}{3} \ln\left(\frac{\bar{a}_1^3 + r_0^3 - a_0^3}{r_0^3}\right) + \frac{2}{3} \ln\left(\frac{\bar{a}_1^3 + r_0^3 - a_0^3}{\bar{a}_2^3 + r_0^3 - a_0^3}\right) \\ & + \frac{2}{3} \ln\left(\frac{\bar{a}_3^3 + r_0^3 - a_0^3}{\bar{a}_2^3 + r_0^3 - a_0^3}\right) + \cdots\end{aligned} \tag{39}$$

For the formulation of the stored energy of volumetric plastic work (37) relation (31) then needs to be replaced by (39).

Note that for an arbitrary history of the plastic volumetric expansion the value of $\vartheta^{\mathrm{p}}(t)$ rises even when the pores shrink. That means by constraint (17) the internal variable $\vartheta^{\mathrm{p}}(t)$ basically measures the ups and downs of pore growth and, therefore, cannot anymore be compared to the monotonic loading. The information about current pore size is in general solely in $J^{\mathrm{p}}(t)$ via relation (26). The corresponding physical constraint is now

$$J^{\mathrm{p}} \geqslant 1, \tag{40}$$

i.e., the pores are not allowed to be smaller than the initial pore size with $J^{\mathrm{p}} = 1$.

4. Comparison of numerical results after 5 temperature steps

The presented material model was employed to study the response of the plated-through vias during thermal cycling. It is common practise to simulate only a few steps of the temperature cycling test and extrapolate the results until fatigue failure is anticipated. Following the traditional approach of, e.g. [1–3,12,22], we apply a temperature history as follows: 456–233–423–233–423–233 K, where 456 K refers to the melting temperature of eutectic SnPb which was assumed to be the stress free state of reference. Note that we apply two forms of loading on the via submodel, the temperature dependent material behavior and the deformation resulting from the global model. Moreover, in order to account for the maximal possible growth of pores within the copper material the irreversibility constraint (17) is applied. Physically speaking this means that we allow the voids to open but not to close irreversibly.

Three (limit) cases are considered.

(1) *Unfilled:* The plated-through vias are empty copper vias embedded in the board as described in Section 2.
(2) *Soft filled:* The copper vias are filled with solder stop mask with material data as outlined in Section 2.
(3) *Hard filled:* The vias are filled with a material harder than copper. We choose here the material parameter of mild steel.

All via positions are analyzed with these three fillings.

Summarizing the results after the temperature changes have been applied we observe that in the cases of no filling and soft filling the vias are – to a different extend – strained mostly in the middle of the copper cylinder. The typical strain distribution is displayed for an unfilled and a soft-filled via of position 4 in Figs. 9 and 10, respectively. In the unfilled via the values of both, plastic strain and volumetric plastic dilatation, i.e., maximal porosity, are smaller than in the filled via. Depending on the position of the unfilled via the maxima of plastic strain and of plastic dilatation occur in the outer region (position 1, 2, 4, 5) as well as in the inner regions (position 3, 6) of the thin copper cylinder, whereas in case of a soft filling the maximum values are all found on the inner side. In that context the wall thickness of the copper cylinder may be of considerable influence and needs to be further investigated.

For hard fillings the location of the maximum straining shifts – as one may expect – away from the copper tube to the attached upper and lower layers, see Fig. 11. Note that because our FEA does not consider debonding of the copper material from the filling the straining that was computed here is not necessarily realistic. The values may differ in particular in case of a loose fitting of a stiff filler, e.g., a wire. This may also prevent bending of the copper tube but it allows for pressure and tension, the main mechanisms that cause pores to grow.

In Table 2 the results are given in detail. Because FEA of the vias at position 1 and 4, and, 2 and 5, respectively, leads to very similar results, we list here only the latter. Moreover, for clarity all values are referred to an average strain and an average dilatation with value 0.03. Note that we compare maximum values and that the position of the maxima may differ. In particular we emphasize that in case of a hard filling the maximum value is on the upper

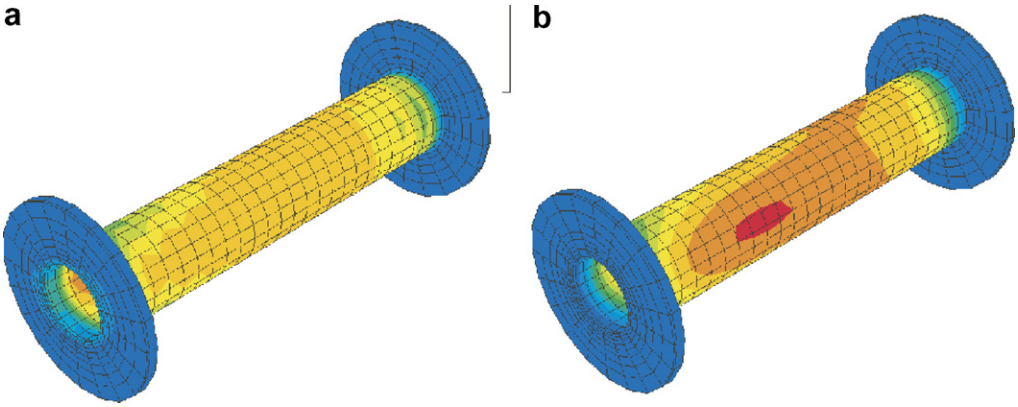

Fig. 9. Distribution of accumulated plastic strain and porosity (as indicated by ε^{p} and ϑ^{p}) in an unfilled via at position 4 after 5 temperature steps (maxima: red, minima: blue): (a) plastic strain ε^{p}; (b) pore growth ϑ^{p}. (For interpretation of the references in color in this figure legend, the reader is referred to the web version of this article.)

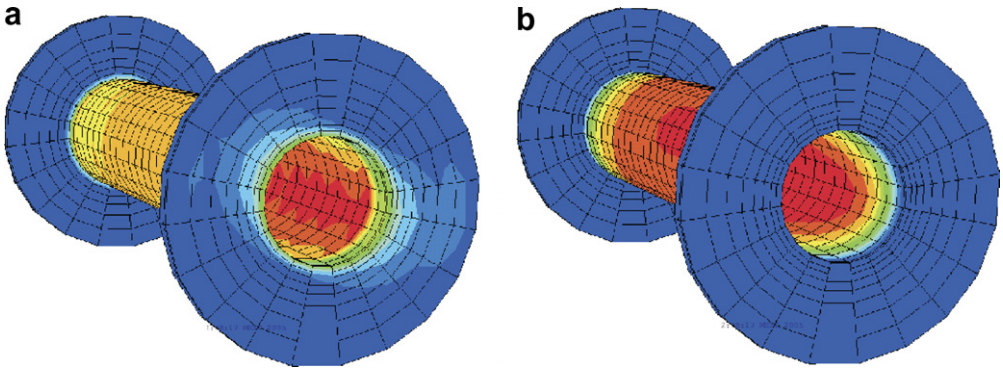

Fig. 10. Distribution of accumulated plastic strain and porosity in a soft-filled via at position 4 after 5 temperature steps (maxima: red, minima: blue): (a) plastic strain ε^{p}; (b) pore growth ϑ^{p}. (For interpretation of the references in color in this figure legend, the reader is referred to the web version of this article.)

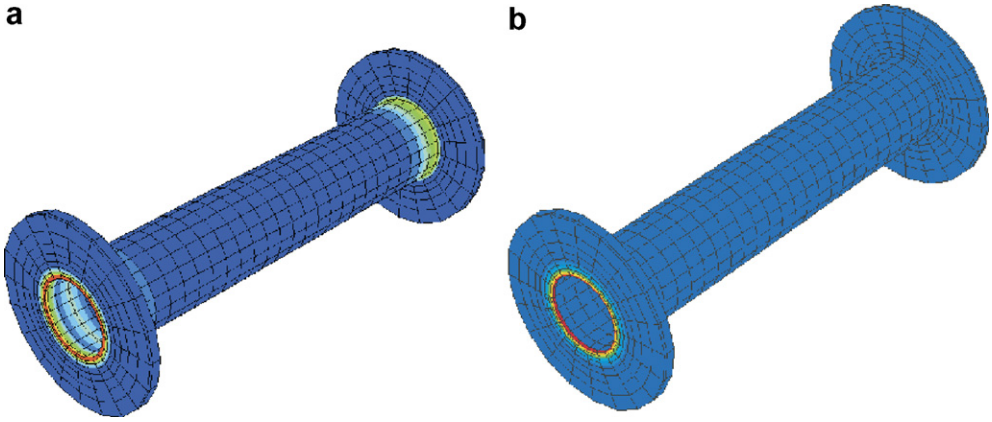

Fig. 11. Typical distribution of accumulated plastic strain and porosity in a hard-filled via after 5 steps (maxima: red, minima: blue): (a) plastic strain ε^{p}; (b) pore growth ϑ^{p}. (For interpretation of the references in color in this figure legend, the reader is referred to the web version of this article.)

boundaries of the via, see Fig. 11. Nonetheless we can summarize as follows:

- The filling of the vias with solder stop mask does not improve necessarily the mechanical properties of the structure. After five temperature changes the unfilled vias show lower plastic strain and lower porosity.
- A hard filling supports the via, i.e, it prevents bending. The maximum of straining is shifted from the center to the boundary of the structure instead.

Table 2
Maxima of plastic strain and pore growth in the different via positions after 5 temperature steps

Via position		Relative strain maximum	Relative dilation maximum
3	No filling	0.8588	0.2905
4		0.9123	0.4183
5		0.8012	0.2859
6		0.8478	0.3095
3	Solder stop mask	1.1223	0.7630
4	filled	1.2328	0.8547
5		1.0567	0.7880
6		1.1088	0.7507
3	Hard filling	1.1687	0.6353
4		1.1757	0.6380
5		1.0737	0.6637
6		1.1128	0.6340

- The via at position 3 (in the middle of the chip) as well as the via at position 4 (on the diagonal) are the most strained ones, and, moreover, show different regimes of loading (stretching, bending). We therefore proceed analyzing only these two positions.

The diagrams in Fig. 12 allow to gain an overview of the development of maximum plastic strain and plastic dilatation in time for the soft-filled vias located at positions 3–6. The response in all positions of the via is similar. The initial cooling 456–233 K causes a formidable plastic strain but no plastic dilatation. The reason for that may be a pressure dominated stress state; because of the different thermal expansion coefficients the copper is bended but under pressure. On the opposite, rising temperature causes tension and voids to grow but – at least in the first steps observed here – no plastic straining. The process repeats with smaller amplitude.

The vias along the diagonals are the most severely strained, all other vias show approximately the same level of strain. In all cases the finite element with the highest absolute value in strain also shows the highest increments in strain after five steps. The analog holds for the plastic dilatation, but the locations of maxima do not coincide.

A similar behavior was observed for the (not displayed) unfilled vias, but here the rising temperature also causes a (comparatively small) growth in plastic strain. Cases where in unfilled vias the element with the highest plastic strain shows saturation already after first cooling, as reported in [2], were not found here. However, in case of the hard-filled vias the temporal development shows these saturation after the first step of cooling for both, plastic strain and pore growth.

5. Long term response

In experiments the number of temperature cycles that a circuit board can tolerate is generally considered to be a measure of the circuit copper's resistance to fatigue damage. It depends in a large part on an inverse relationship with strain amplitude $\Delta\varepsilon$ within one cycle. The fatigue failure of a metal, as here the electrodeposited copper, is commonly estimated using a Coffin–Manson relationship of the form [4]

$$\frac{\Delta\varepsilon}{2} = \frac{\sigma_f}{E}(2N_f)^b + \varepsilon_f(2N_f)^c, \tag{41}$$

where $(2N_f)$ is the number of strain reversals (cycles), E is Young's modulus, σ_f is the tensile strength, and ε_f is the related ductility. The exponents b, c are empirical constants.

Fatigue of copper is characterized by elastic and plastic strain components. During a high-strain/low-cycle testing as considered here the dominant component is the plastic deformation. Elastic deformations play a role mainly during low-strain/high-cycle testing, therefore, the region of elastic deformation is also considered as the dynamic region. In that case the first term of Eq. (41) dominates and fatigue performance is mainly a function of the tensile strength.

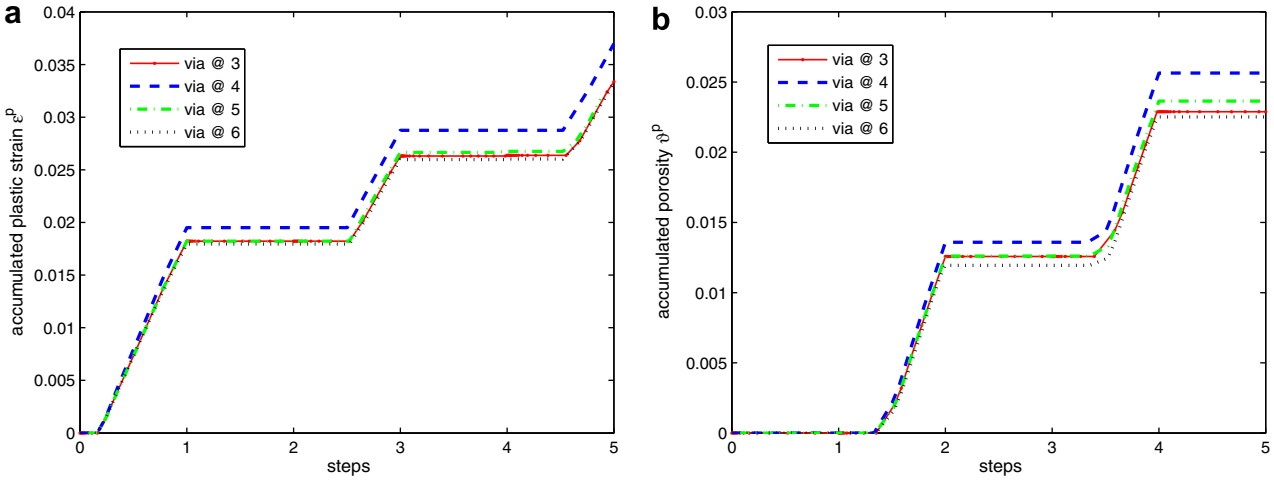

Fig. 12. Temporal development of the maxima of plastic strain and pore growth in the soft-filled via: (a) plastic strain; (b) pore growth.

Conversely, in the high-strain/low-cycle regime, the second term of (41) dominates and fatigue is a function of ductility. The account in terms of stress is less useful and the first term in Eq. (41) does not apply. The strain amplitude within one cycle is replaced by the plastic strain increment to give

$$\frac{\Delta\varepsilon^{\mathrm{p}}}{2} = \varepsilon_{\mathrm{f}}(2N_{\mathrm{f}})^{c}, \tag{42}$$

where c is known as the fatigue ductility exponent, commonly ranging from -0.5 to -0.7 for metals. Different sources report that the ductility of electrodeposited copper is smaller than the ductility of bulk copper, [3,13,17,8]. Thus, we assume here a maximal ductility of 20%.

We now apply relation (42) to the results of Section 4. The plastic strain increment is found by averaging the plastic strain from step 2 to step 5. The first step is skipped because the strain induced by the initial cooling gives no information about a typical strain increment.

The region with maximum straining of the via is marked in Figs. 13 and 14 by a circle. Here we get (averaged over the integration points of the element) for the unfilled via at position 4 $\Delta\varepsilon^{\mathrm{p}}_{\mathrm{ave}} = 0.005737$ and for the soft-filled via $\Delta\varepsilon^{\mathrm{p}}_{\mathrm{ave}} = 0.002876$. Applying Eq. (42) gives a live expectation of $N_{\mathrm{f}} = 591$ and $N_{\mathrm{f}} = 1867$ for the unfilled and filled via, respectively. The same procedure applied to the vias at position 3 results in $N_{\mathrm{f}} = 1084$ for the unfilled and $N_{\mathrm{f}} = 525$ for the filled via.

The calculated numbers of cycles are low with respect to the required life expectation of at least 4000 cycles, i.e., $N_{\mathrm{f}} = 8000$. Moreover, this approach does not account for the fact that the absolute value of ε^{p} is higher in case of a filling in the vias. Also, additional information about crack or pore growth are not consulted for life time estimation.

To answer the question of how reliable this simple traditional approach is, we study in the following the mechanical response of the vias over a longer period of time and analyze the plastic strain as well as the expected pore growth. To this end, 20 steps of temperature cycling after the initial cooling are computed. Because of the significant computational effort we analyze here only the maximal loaded vias at position 3 and 4, the conclusion for the remaining via positions are analogous. In case of the hard-filled vias we do not observe additional straining after the first cool down. Therefore, and because hard filling is of

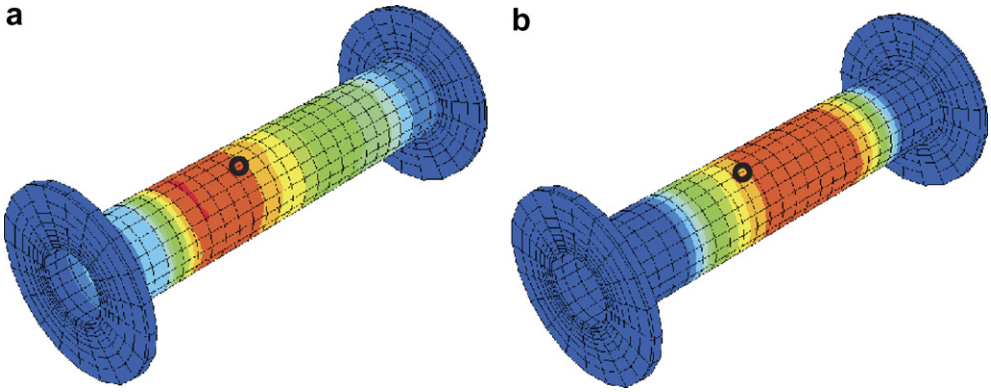

Fig. 13. Distribution of accumulated plastic strain and porosity in an unfilled via at position 3 (maxima: red, minima: blue): (a) plastic strain; (b) volumetric plastic dilatation. (For interpretation of the references in color in this figure legend, the reader is referred to the web version of this article.)

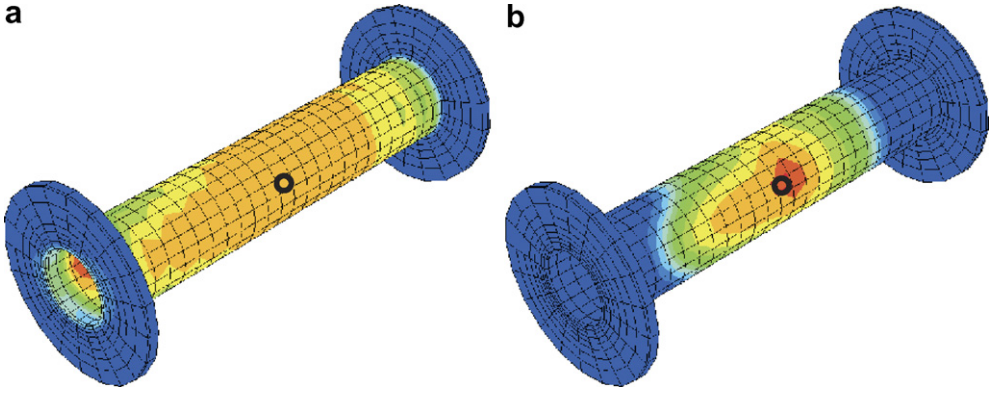

Fig. 14. Distribution of accumulated plastic strain and porosity in an unfilled via at position 4 (maxima: red, minima: blue): (a) plastic strain; (b) volumetric plastic dilatation. (For interpretation of the references in color in this figure legend, the reader is referred to the web version of this article.)

somewhat artificial nature, we investigate in the following only the unfilled and soft-filled vias.

The distribution of plastic variables after 21 temperature steps is shown in Figs. 13 and 14 for vias at position 3 and 4, respectively. During continued temperature cycling the location of the maximal values of plastic strain and plastic pore growth changes. The displayed distribution nicely reflects the loading of the via. In position 4 bending dominates and the accumulated plastic strain and, in particular, the plastic volumetric dilatation show a localization on the corresponding sides of the via. In position 3 (direct underneath the chip) the via is mainly stretched along its axis and the distribution of plasticity in circumferential direction is basically homogeneous. The highest plastic straining is accumulated in the upper half of the copper tube, whereas the pores and voids grow increasingly towards the lower half. If we consider superposition of both defects there seems to be a higher probability of failure within the middle parts of the vias. Clearly, here is some need to substantiate such an effect experimentally, for a first indication see Fig. 7.

The strain values at inner and outer side of the via wall become similar. Moreover, starting after about 8 steps the rising of temperature starts to cause a small increase in plastic strain also for the soft-filled vias. Pore growth as modelled here can only happen in a tension dominated state, i.e., during heating.

To account for both plastic straining and increasing porosity the temporal development of the plastic variables is plotted in the Figs. 15–18 for the position marked in Fig. 14. The values computed at this locus are close to the absolute maxima of ε^{p}, ϑ^{p} for all analyzed vias. In order to additionally avoid numerical artifacts all plotted values are averaged within the finite elements.

For all studied vias the cooling from manufacturing temperature of 456 K down to 233 K initiates an formidable amount of plastic strain with amplitudes higher in the filled than in the unfilled vias. Within the next temperature

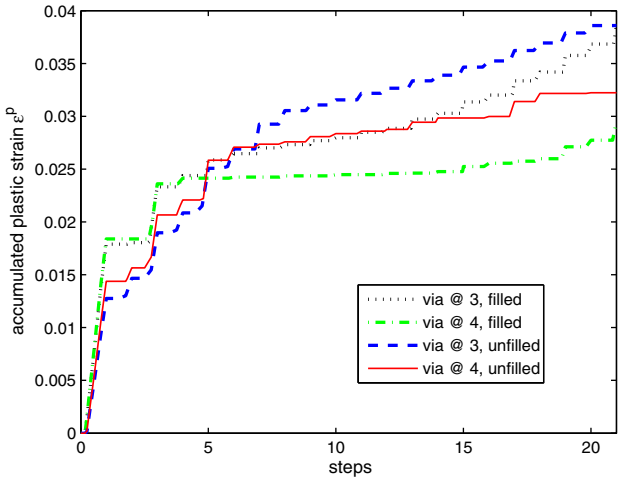

Fig. 15. Temporal development of plastic straining within 21 temperature steps for unfilled and soft-filled vias.

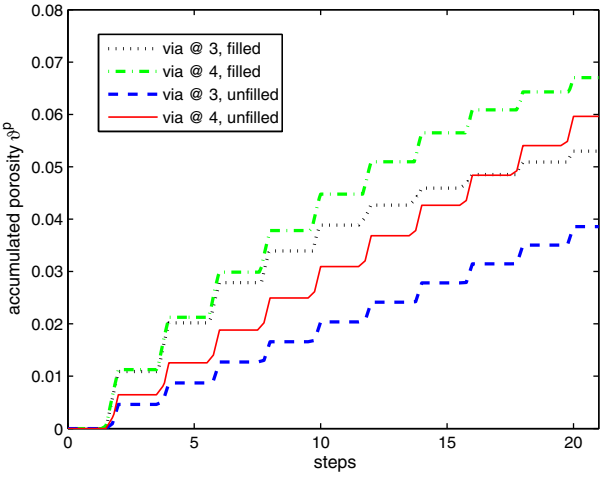

Fig. 17. Temporal development of monotonically assumed void growth within 21 temperature steps for unfilled and soft-filled vias.

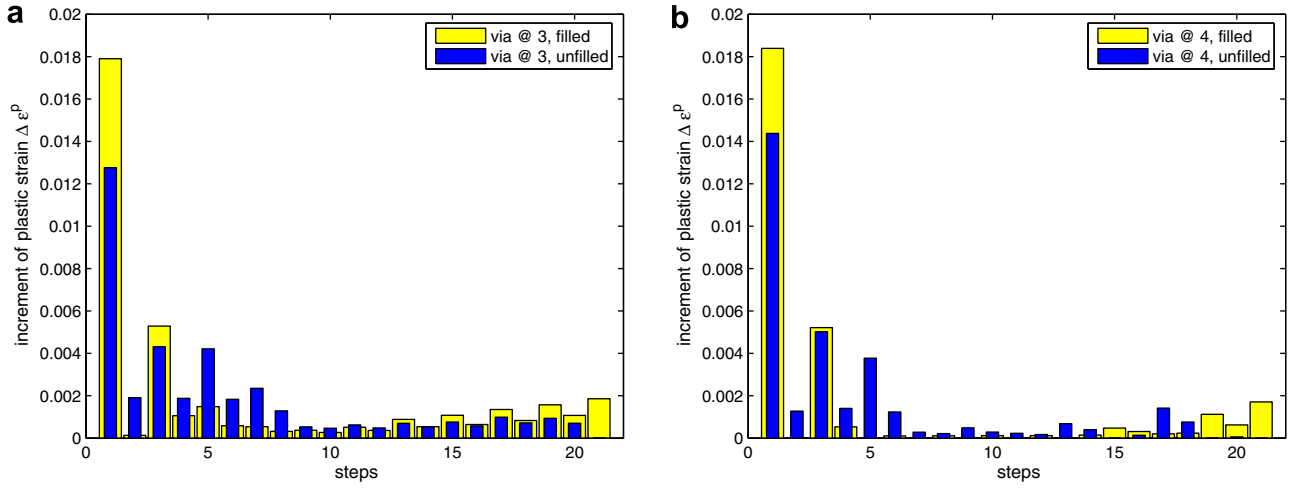

Fig. 16. Increments of plastic strain $\Delta\varepsilon^{p}$ within the temperature steps for unfilled and soft-filled vias: (a) vias at position 3; (b) vias at position 4.

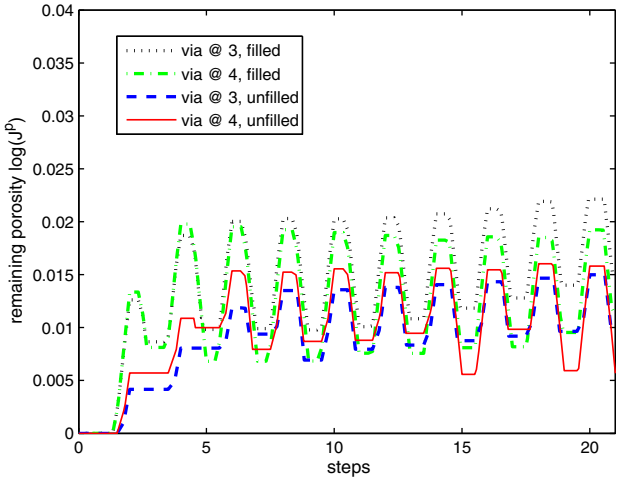

Fig. 18. Temporal development of pore opening and closure within 21 temperature steps for unfilled and soft-filled vias.

steps the increments of plastic strain are still large but around step 6 the plastic straining shows saturation. Then it depends on the position of the via how much the strain increments reduces. To illustrate this, Fig. 16 shows the strain increments within the steps. We clearly see that the increment of plastic strain computed from a FEA of 5 temperature steps is not representative for the rest of the life cycle. The increment $\Delta\varepsilon^{\mathrm{p}}$ is in the first steps significantly higher than the average between step 6 and 21. In particular, the influence of the fillings in the vias is inverse. In case of no filling we get in position 4 an average strain of $\Delta\varepsilon^{\mathrm{p}}_{\mathrm{ave}} = 0.000798$ (with filling $\Delta\varepsilon^{\mathrm{p}}_{\mathrm{ave}} = 0.000664$), resulting in $N_{\mathrm{f}} = 15{,}818$ and $N_{\mathrm{f}} = 21{,}490$, respectively. The corresponding numbers of the unfilled and filled via at position 3 are $N_{\mathrm{f}} = 4529$ and $N_{\mathrm{f}} = 4942$. Note that the computed live expectations are by an order of magnitude larger than above.

Fig. 17 displays the temporal development of the maximal possible void growth, i.e., the volumetric plastic dilatation ϑ^{p}. Nearly constant increments $\Delta\vartheta^{\mathrm{p}}$ are observed after each heating step. Because the volumetric plastic dilatation as a function of time (or steps) shows an almost linear slope it may reach a critical value after a certain number of steps. Ductile metals are known to fail by fracture when the porosity reaches a volume fraction of at most 0.3, [19]. Extrapolating the function in Fig. 17, this critical porosity would be reached after 150...300 temperature steps. This number is a not necessarily realistic because by Eq. (17) we allow the pores to open in tension but not to shrink in compression. Consequently, ϑ^{p} can be considered an auxiliary value which at best gives an upper limit for the realistic porosity.

Henceforth, lets follow the constitutive model outlined in Section 3 which allows also for pore closure. To this end, we introduce the variable $\tau^{\mathrm{p}} = \ln(J_{\mathrm{p}})$ to measure plastic volume change, i.e., to account for the growth and shrinkage of voids and keep ϑ^{p} to be an internal variable accounting for volumetric plasticity and for work hardening but now without its physical meaning of pore growth. To ensure that the pores must not get smaller than their initial size within the virgin material we constrain $\tau^{\mathrm{p}} \geqslant 0$.

Table 3
Life expectation in the different via positions

Via position		$N_{\mathrm{f}}(\varepsilon^{\mathrm{p}})$	$N_{\mathrm{f}}(\tau^{\mathrm{p}})$
3	No filling	4529	1293
3	Soft-filling	4942	1864
4	No filling	15,818	6172
4	Soft-filling	21,490	14,125

Fig. 18 monitors the volumetric growth (and shrinkage) in the vias during 21 temperature steps. In all vias the first heating steps cause a significant growth in porosity. Then, similar to the plastic straining, a certain saturation is reached after approximately six steps. Thenceforward pores in the copper material open and close with every temperature cycle. The resulting porosity shows a slight increase in every cycle.

To estimate the life time of a materials from its porosity an empirical equation like (41) is not known. Therefore we apply the following strategy to calculate the number of cycles when the resulting porosity reaches a critical value. First we determine the porosity after the first few cycles, here we choose step 6. For the unfilled via at position 3 we get $\tau^{\mathrm{p}}_{\mathrm{ini}} = 1.187 \times 10^{-4}$, for the filled via $\tau^{\mathrm{p}}_{\mathrm{ini}} = 2.003 \times 10^{-4}$. Now we compute the average increase of porosity within every temperature cycle from step 6 to 21 ($\Delta\tau^{\mathrm{p}} = 1.499 \times 10^{-4}/\Delta\tau^{\mathrm{p}} = 2.2135 \times 10^{-4}$) and extrapolate that increase in a linear manner until the resulting porosity reaches the critical value.

$$\Delta\tau^{\mathrm{p}} = \left(\tau^{\mathrm{p}}_{\mathrm{crit}} - \tau^{\mathrm{p}}_{\mathrm{ini}}\right) N_{\mathrm{f}}^{-1}. \tag{43}$$

The number of cycles ($2N_{\mathrm{f}}$) corresponds to the life expectation. Table 3 summarizes the results for both, plastic straining and resulting porosity computed with 21 temperature steps. Both criteria yield qualitatively equal results and show the unfilled via at position 3 being the most likely to fail. The lower numbers for the porosity criterion is likely to be caused by the linear way of extrapolation (Eq. (43) vs. Eq. (42)). Fillings support the vias, in particular, in a tension-compression dominated state. An experimental verification of the observed correlations (as well as of the relatively high fatigue ductility) was not available to us and is left for future research.

6. Conclusions

The presented analysis of plated trough vias shows that both mechanisms, plastic straining and the growth of pores within the copper via have an essential influence on the life time expectation of the vias and, consequently, the whole circuit unit. The actual accumulated damage is determined by the position of the via on the PC board and by its filling. To estimate the life expectation not only the plastic straining but also the growth of voids should be investigated. For the latter we presented a simple engineering model of dilute

void growth which captures the growing porosity in the copper via in a qualitatively correct manner. This porous plastic model presents a workable set of constitutive equations and is open to further (micromechanically motivated) improvements.

The extrapolated number of cycles until failure of the units depends on the number of temperature cycles considered in the numerical analysis. In particular, a realistic life time estimate needs to base on a finite element analysis of at least 20 temperature steps. Considering less steps gives rather accidental results influenced, e.g., by the initial reference state. Furthermore, after few temperature cycles it is not yet possible to estimate whether the filling of a copper via supports plastic straining or prevents it.

Presumed that the input to the finite element analysis, in particular the material properties of the electrolytically deposited copper and the failure criteria, reflect the actual situation, the introduced FEA-based strategy can serve as a predictive tool for the plated through holes and vias. This reduces the need of highly repetitive and costly experimental failure tests, resulting in significant cost savings to the industry.

Acknowledgement

The authors are grateful to P. Werdin, TU Berlin, for adapting the material subroutines to the finite element system ABAQUS.

Appendix

In Tables 4–7 the mechanical and thermal parameter of the FCOB circuit unit are summarized. The temperature dependency is interpolated linearly.

Table 4
Material data of orthotropic FR4 material

T (K)	E_x, E_y (MPa)	E_z (MPa)	ν_{xy}	ν_{xz}, ν_{yz}	G_{xy} (MPa)	G_{xz}, G_{yz} (MPa)
223	14,218	7109	0.15	0.4	6182	2539
298	13,116	6558	0.15	0.4	5703	2342
373	12,166	6083	0.15	0.4	5290	2172
423	11,225	5613	0.15	0.4	4880	2005
433	10,568	5284	0.15	0.4	4595	1887
443	9277	4638	0.15	0.4	4033	1656
453	5241	2620	0.15	0.4	2279	935
461	3038	1519	0.15	0.4	1320	542

Table 5
Elasticity, initial yield stress and reference plastic strain of electrolytically deposited copper (cf. Section 3, data of [5])

T (K)	E (MPa)	ν	σ_{y_0} (MPa)	ε_0^p
208	45,086	0.34	156	0.00346
293	43,823	0.34	149	0.00340
393	43,994	0.34	146	0.00333
473	39,285	0.34	121	0.00308
573	31,028	0.34	87.5	0.00282

Table 6
Elastic parameter of solder stop mask and soft filling

T (K)	E (MPa)	ν
218	6000	0.34
295	5000	0.38
343	3400	0.40
373	2500	0.42
423	1000	0.45

Table 7
Thermal expansion coefficients

	$\alpha_x = \alpha_y$ (ppm/K)	α_z (ppm/K)
FR4 board	1.7×10^{-5}	6×10^{-5}
Copper	1.76×10^{-5}	1.76×10^{-5}
Solder stop mask	6×10^{-5}	6×10^{-5}
Filling	6×10^{-5}	6×10^{-5}

References

[1] Albrecht HJ, Jendry J, Müller WH, Wieand C. Lebensdauervorhersagen für Vias und Mikrovias in HDI-Boards per FE-Simulation und ihre experimentelle Verifikation. In: Wolter KJ, Wiese S, editors. Interdisziplinäre Methoden in der Aufbau-und Verbindungstechnik. ddp goldenbogen: Dresden; 2003.

[2] Albrecht HJ, Jendry J, Müller WH, Wieand C. Lifetime prediction by fe-simulation and experimental verification for vias and microvias in HDI-substrates. In: Proc. of eighth Ann. Pan Pacific microelectronic symposium (SMTA), Hawai; 2003. p. 201–8.

[3] Barker DB, Dasgupta A. Thermal analysis in plated-through-hole reliability. In: Lau JH, editor. Thermal stress and strain in microelectronic packaging. New York: van Nostrand Reinhold; 1993.

[4] Beitz W, Küttner KH. Dubbel-Taschenbuch für den Maschinenbau. Springer-Verlag; 1990.

[5] DiTomasso JC. Stress analysis of vias within general electric's multichip modules. University of Massachusetts at Amherst, MA, report provided on the web, http://www.ecs.umass.edu/mie/labs/mda/fea/ditomaso/Main.htm; 2000.

[6] Fiori V, Zhang X, Tee TY. Multi-level numerical analysis on the reliability of Cu/low-k interconnection in FCBGA package. In: Proceedings of the 7th electronics packaging technology conference, Proc. EPTC, Singapore; 2005. p. 188–95.

[7] Gologanu M, Leblond JB, Perrin G, Devaux J. Theoretical models for void coalescence in porous ductile solids. I. coalescence "in layers". Int J Solids Struct 2001;38(32–33):5581–94.

[8] Hayes C. Characterization of electrodeposited copper for dynamic flex applications (part 2). INSIGHT, Int Disk Drive Equip Mater Assoc 2001;3–4:34–6.

[9] Lu L, Schwaiger R, Shan ZW, Dao M, Lu K, Suresh S. Nano-sized twins induce high rate sensitivity of flow stress in pure copper. Acta Mater 2005;53:2169–79.

[10] Miehe C. Exponential map algorithm for stress updates in anisotropic multiplicative elastoplasticity for single crystals. Int J Numer Method Eng 1996;39(19):3367–90.

[11] Müller WH, Albrecht H-J, Hyslop DC, Jendry J, Ng KMW, Tan KH. Modelling the reliability of high-density substrates and associated microelectronic components. In: Proceedings of the 3rd electronics packaging technology conference (EPTC); 2000. p. 412–8.

[12] Müller WH, Jendry J. Zwischenbericht, Siemens, ZT MF6 (in German). TU Berlin: Institute of Mechanics; 2002.

[13] Niewczas M, Embury JD. Approaching the theoretical strength in ductile copper. In: Zabaras et al. editors. The integration of material, process and product design; 1999.

[14] Nucci JA, Keller RR, Field DP, Shacham-Diamond Y. Grain boundary misorientation angles and stress-induced voiding in oxide passivated copper interconnects. Appl Phys Lett 1997;70:1242–4.
[15] Ortiz M, Molinari A. Effect of strain hardening and rate sensitivity on the dynamic growth of a void in a plastic material. Trans ASME 1992;59:48–53.
[16] Ortiz M, Stainier L. The variational formulation of viscoplastic constitutive updates. Comput Method Appl Mech Eng 1999;171(3–4):419–44.
[17] Read DT, Cheng Y-W, Geiss R. Mechanical behavior of electrodeposited copper film at elevated temperatures. Talk at ASME IMECE 2004, Anaheim, CA, November 15, 2004.
[18] Schiotz J, Vegge T, Di Tolla FD, Jacobsen KW. Atomic-scale simulations of the mechanical deformation of nanocrystalline metals. Phys Rev B 1999;60:11971.
[19] Tvergaard V. Material failure by void growth to coalescence. Adv Appl Mech 1990;27:83–153.
[20] Weinberg K. Material models of microstructured solids – theory, numeric and applications. Habilitationsschrift, TU Berlin; 2006.
[21] Weinberg K, Mota A, Ortiz M. A variational constitutive model for porous metal plasticity. Comput Mech 2006;37(2):142–52.
[22] Wunderle B, Dudek R, Michel B, Reich H. Thermo-mechanical reliability of power flip-chip cooling concepts. In Proceedings of the electronic components and technology conference, IEEE; 2004. p. 427–37.